

FAST CONVOLUTION-BASED METHODS FOR COMPUTING THE SIGNED DISTANCE FUNCTION AND ITS DERIVATIVES

KARTHIK S. GURUMOORTHY ^{§*}, ANAND RANGARAJAN ^{§†}, AND MANU SETHI ^{§‡}

Abstract. We present a fast convolution-based technique for computing an approximate, signed Euclidean distance function at a set of 2D and 3D grid locations. Instead of solving the non-linear static Hamilton-Jacobi equation ($\|\nabla S\| = 1$), our solution stems from solving for a scalar field ϕ in a *linear* differential equation and then deriving the solution for S from its exponent. In other words, when S and ϕ are related by $\phi = \exp(-\frac{S}{\tau})$ and ϕ satisfies a specific linear differential equation corresponding to the extremum of a variational problem, we obtain the Euclidean distance function $S = -\tau \log(\phi)$ in the limit as $\tau \rightarrow 0$. This is in sharp contrast to solvers such as the fast marching and fast sweeping methods which directly solve the Hamilton-Jacobi equation by the Godunov upwind discretization scheme. Our linear formulation provides us with a closed-form solution to the approximate Euclidean distance function expressed as a discrete convolution, and hence efficiently computed by the Fast Fourier Transform (FFT). Moreover, the solution circumvents the need for spatial discretization of the derivative operator thereby providing highly accurate results. As $\tau \rightarrow 0$, we show the convergence of our results to the true solution and also bound the error for a given value of τ . The differentiability of our solution allows us to compute—using a set of convolutions—the first and second derivatives of the approximate distance function. In order to determine the sign of the distance function (defined to be positive inside a closed region and negative outside), we compute the winding number in 2D and the topological degree in 3D and again explicitly show that these computations can be performed via fast convolutions. We demonstrate the efficacy of our method through a set of experimental results.

AMS subject classifications. Primary 65D99, 35J05; Secondary 35J08

1. Introduction. Euclidean distance functions (more popularly referred to as distance transforms) are widely used in image analysis and synthesis [12]. The task here is to assign at each grid point a value corresponding to the Euclidean distance to its nearest neighbor from a given point-set. Formally stated: given a point-set $Y = \{Y_k \in \mathbb{R}^D, k \in \{1, \dots, K\}\}$ where D is the dimensionality of the point-set and a set of equally spaced Cartesian grid points X , the Euclidean distance function problem requires us to assign

$$S(X) = \min_k \|X - Y_k\| \quad (1.1)$$

where $\|\cdot\|$ represents its Euclidean norm. In computation geometry, this is the Voronoi problem [6] and the solution $S(X)$ can be visualized as a set of cones with the centers being the point-set locations $\{Y_k\}$. The Euclidean distance function problem is a special case of the eikonal equation where the forcing function is identically equal to 1 everywhere and hence satisfies the differential equation

$$\|\nabla S\| = 1, \quad (1.2)$$

barring the point-set locations and the Voronoi boundaries where it is not differentiable. Here $\nabla S = (S_x, S_y)$ denotes the gradients of S . This is a nonlinear differential equation and an example of a static Hamilton-Jacobi equation.

*Email: sgk@ufl.edu

†Email: anand@cise.ufl.edu

‡Email: msethi@cise.ufl.edu

[§]Department of Computer and Information Science and Engineering, University of Florida, Gainesville, Florida, USA

Since the advent of the fast marching method [13, 12], the literature is replete with pioneering works which have successfully tackled this problem. Fast marching is an elegant technique which solves for S in $O(N \log N)$ time at the given N grid locations using the Godunov upwind discretization scheme. Faster methods like the fast sweeping method [20] employs Gauss-Seidel iterations and solves for S in $O(N)$. The ingenious work in [19] gives an $O(N)$ implementation of the fast marching method with a cleverly chosen *untidy priority queue* data structure. Fast sweeping methods have also been extended to the more general static Hamilton-Jacobi equation [11] and also for the eikonal equation on non-regular grids [9, 10]. A Hamiltonian approach to solve the eikonal equation can be found in [16].

The intriguing aspect of our method is that a nonlinear Hamilton-Jacobi equation is obtained in the limit as $\tau \rightarrow 0$ of a linear equation. When the distance function S is expressed as the exponent of a scalar field ϕ , specifically $\phi(X) = \exp\left(\frac{-S(X)}{\tau}\right)$, and if $\phi(X)$ is the solution to a variational problem satisfying its corresponding linear Euler-Lagrange equation, we show that as $\tau \rightarrow 0$, S satisfies Equation 1.2. Consequently, instead of solving the non-linear Hamilton-Jacobi equation, one can solve for the function ϕ (taking advantage of its linearity), and then compute an approximate S for small values of τ . This computational procedure would be approximately equivalent to solving the original Hamilton-Jacobi equation. Our linear approach results in a closed-form solution, which can be expressed as a discrete convolution and computed in $O(N \log N)$ time using a Fast Fourier Transform (FFT) [3] where N is the number of grid points. This is major advantage of our method as the closed-form solution circumvents the need for spatial discretization of the derivative operator in Equation 1.2, a problem that permeates the Hamilton-Jacobi solvers [13, 12, 20]. This accounts for improved accuracy of our technique. However, a minor caveat of our method being that the resultant Euclidean distance function is an approximation since it is obtained for a small but non-zero value of τ , but nevertheless converges to the true solution as $\tau \rightarrow 0$.

The linear approach gives us an unsigned distance function. We complement this by independently finding the sign of the distance function in $O(N \log N)$ time on a regular grid in $2D$ and $3D$. We achieve this by computing the *winding number* for each location in the $2D$ grid and its equivalent concept, the *topological degree* in $3D$. We show that just as in the case of the unsigned Euclidean distance function, the winding number and the topological degree computations can also be written in closed-form, expressed as discrete convolutions and efficiently computed using FFTs. We are not cognizant of any previous work that uses the winding number and topological degree approaches to compute signed distance functions. Very often, we also seek the gradient of the signed distance function which are not easy to obtain via the Hamilton-Jacobi solvers due to the lack of differentiability of their solution. Since our method results in a differentiable closed-form solution, we can leverage it to compute these quantities. Surprisingly we noticed that the solution for the gradients too can be written as discrete convolutions and efficiently computed using FFTs. Furthermore, they can also be shown to converge to their true value as $\tau \rightarrow 0$. To our knowledge, fast computation of the derivatives of the distance function on a regular grid using discrete convolutions is new.

The paper is organized as follows. In Section 2 we derive the linear equation formalism for the Euclidean distance function problem and show convergence of our solution to the true solution as $\tau \rightarrow 0$. We provide an approximate closed-form solution to compute the distance function and give an error bound between the computed

and true distance functions for a given value of τ . Section 3 demonstrates how the closed-form solution can be represented as a convolution and thus efficiently computed using fast Fourier transforms. In Sections 4 and 5, we compute the winding number (in 2D), the topological degree (in 3D) and the derivatives of the distance function, by again expressing these quantities using discrete convolutions. In Section 6, we show anecdotal evidences for the usefulness of our method by furnishing both experimental results and comparisons to standard techniques. We finally conclude in Section 7.

2. Linear equation approach for Euclidean distance functions. Consider a variational problem

$$I(\phi) = \tau^2 \int \|\nabla \phi\|^2 dX + \int |\phi - \phi_0^\tau|^2 dX \quad (2.1)$$

where ϕ_0^τ —a function of τ —represents the initial wave front concentrated around the source locations $\{Y_k\}_{k=1}^K$ in the as $\tau \rightarrow 0$. We define $\phi_0^\tau(X)$ as

$$\phi_0^\tau(X) = \sum_{k=1}^K \phi_k^\tau(X) \quad (2.2)$$

where $\phi_k^\tau(X)$ is chosen such that it is *square integrable* to 1 with its support sequentially converging towards the point source Y_k as τ approaches zero and asymptotically behaves like the square-root of a δ function centered around Y_k . The square integrability to 1 constraint changes its functional form in accordance with the spatial dimension, as explicated in the subsequent sections.

The Euler-Lagrange equation corresponding to the extremum of $I(\phi)$ computed over the scalar field ϕ is given by the *linear* equation

$$-\tau^2 \nabla^2 \phi + \phi = \phi_0^\tau, \quad (2.3)$$

where ∇ stands for the Laplacian operator. We may be tempted to replace ϕ_0^τ in Equation 2.3 with a combination of delta functions each centered around Y_k and obtain an *inhomogeneous screened Poisson* partial differential equation. But since the delta functions are not square-integrable, they cannot be incorporated into the variational framework given in Equation 2.1. Defining ϕ_0^τ as in Equation 2.2 forces it to behave like the square-root of a δ function as $\tau \rightarrow 0$ and hence is square-integrable for all values of τ .

To our amazement, we realized that when we relate $\phi(X) = \exp\left(\frac{-S(X)}{\tau}\right)$ and ϕ satisfies Equation 2.3, S asymptotically satisfies the Hamilton-Jacobi equation 1.2 in the limit $\tau \rightarrow 0$, as elucidated under Section 2.2. This relationship motivates us to solve the linear equation 2.3 instead of the non-linear eikonal equation and then compute the distance function via

$$S(X) = -\tau \log \phi(X). \quad (2.4)$$

2.1. Solution for the Euclidean distance function. We now derive the solution for $\phi(X)$ (in 1D, 2D and 3D) satisfying Equation 2.3 and then for $S(X)$ from the relation 2.4.

Since it is meaningful to assume that $S(X)$ approaches infinity for points at infinity, we can use Dirichlet boundary conditions $\phi(X) = 0$ at the boundary of an

unbounded domain. Using a Green's function approach [2], we can write expressions for the solution ϕ . The Green's function G satisfies the relation

$$(-\tau^2 \nabla^2 + 1)G(X) = -\delta(X). \quad (2.5)$$

The form of the solution for G [2] in 1D, 2D and 3D over an unbounded domain with vanishing boundary conditions at ∞ is given by,

1D:

$$G(X) = \frac{1}{2\tau} \exp\left(\frac{-|X|}{\tau}\right). \quad (2.6)$$

2D:

$$\begin{aligned} G(X) &= \frac{1}{2\pi\tau^2} K_0\left(\frac{\|X\|}{\tau}\right) \\ &\approx \frac{\exp\left(\frac{-\|X\|}{\tau}\right)}{2\tau\sqrt{2\pi\tau\|X\|}}, \quad \frac{\|X\|}{\tau} \gg 0.25 \end{aligned} \quad (2.7)$$

where K_0 is the modified Bessel function of the second kind.

3D:

$$G(X) = \frac{1}{4\pi\tau^2} \frac{\exp\left(\frac{-\|X\|}{\tau}\right)}{\|X\|}. \quad (2.8)$$

The solution for ϕ can then be obtained via convolution as

$$\phi(X) = G(X) * \phi_0^\tau(X) = \sum_{k=1}^K G(X) * \phi_k^\tau(X) \quad (2.9)$$

from which S can be recovered using the mathematical relation 2.4.

2.2. Proofs of convergence. We now prove that as $\tau \rightarrow 0$, $S(X)$ —obtained from the exponent of ϕ which satisfies Euler-Lagrange equation refeq:phiEquationwithtau—converges to the true solution $r(X) = \min_k \|X - Y_k\| = \|X - Y_{k_0}\|$. We show this explicitly for each spatial dimension.

1D: Since we require $\phi_k^\tau(X)$ to behave like a square-root of the δ function centered at Y_k as $\tau \rightarrow 0$, we define it as

$$\phi_k^\tau(X) = \begin{cases} \frac{1}{\sqrt{\tau}} & \text{for } Y_k - \frac{\tau}{2} \leq X \leq Y_k + \frac{\tau}{2}; \\ 0 & \text{otherwise} \end{cases}$$

Plugging it in Equation 2.9 and using the expression for the 1D Green's function, we solve for ϕ as

$$\phi(X) = \frac{1}{2\tau^{\frac{3}{2}}} \sum_{k=1}^K \int_{X - Y_k - \frac{\tau}{2}}^{X - Y_k + \frac{\tau}{2}} \exp\left(\frac{-|Z|}{\tau}\right) dZ. \quad (2.10)$$

Using the relation (2.4), the Euclidean distance function is given by

$$S(X) = C_\tau - \tau \log\left(\sum_{k=1}^K \int_{B_k^\tau(X)} \exp\left(\frac{-|Z|}{\tau}\right) dZ\right), \quad (2.11)$$

where $C_\tau = \tau \log(2) + \frac{3}{2}\tau \log(\tau)$ and the integration region $\mathcal{B}_k^\tau(X)$ equals

$$\mathcal{B}_k^\tau(X) = \left[X - Y_k - \frac{\tau}{2}, X - Y_k + \frac{\tau}{2} \right]. \quad (2.12)$$

In order to show convergence to $r(X)$ as τ approaches zero, we define

$$\alpha_k \equiv \begin{cases} 1 & \text{if } X > Y_k; \\ -1 & \text{if } X < Y_k \end{cases}$$

for each k . Then for sufficiently small τ we get

$$\begin{aligned} S(X) &\leq C_\tau - \tau \log \left\{ \tau \exp \left(\frac{-|X - Y_{k_0} + \alpha_{k_0} \frac{\tau}{2}|}{\tau} \right) \right\} \\ &= C_\tau - \tau \log(\tau) + \left| X - Y_{k_0} + \alpha_{k_0} \frac{\tau}{2} \right|. \end{aligned} \quad (2.13)$$

as $|X - Y_{k_0} + \alpha_{k_0} \frac{\tau}{2}| \geq |Z|$ for $Z \in \mathcal{B}_{k_0}^\tau$.

On the other hand, since $|X - Y_k - \alpha_k \frac{\tau}{2}| \leq |Z|, \forall Z \in \mathcal{B}_k^\tau$ at small values of τ , we also get

$$\begin{aligned} S(X) &\geq C_\tau - \tau \log \left\{ \tau \sum_{k=1}^K \exp \left(\frac{-|X - Y_k - \alpha_k \frac{\tau}{2}|}{\tau} \right) \right\} \\ &\geq C_\tau - \tau \log(\tau) - \tau \log \left\{ K \exp \left(\frac{-|X - Y_{k_0} - \alpha_{k_0} \frac{\tau}{2}|}{\tau} \right) \right\} \\ &= C_\tau - \tau \log(\tau) - \tau \log(K) + \left| X - Y_{k_0} - \alpha_{k_0} \frac{\tau}{2} \right|. \end{aligned} \quad (2.14)$$

In order to see why the second step in the above relation holds, consider the two scenarios (i) X lies on the Voronoi boundary and (ii) X is not a point on the Voronoi boundary. If X doesn't lie on the Voronoi boundary, then exist a neighborhood $N_p(X)$ around X such that $\forall Y \in N_p(X), |Y - Y_{k_0}| < |Y - Y_k|, \forall k$. Since $|X - \alpha_{k_0} \frac{\tau}{2}| \in N_p(X)$ for sufficiently small values of τ , the aforementioned relation is true. On the flip side if X is a point on the Voronoi boundary, the closest source point Y_k is not uniquely defined. However we can unambiguously choose a source point Y_{k_0} and a τ_0 such that for $\tau \in (0, \tau_0]$, $|X - \alpha_{k_0} \tau - Y_{k_0}| < |X - \alpha_k \tau - Y_k|, \forall k$ and $|X - Y_{k_0}| \leq |X - Y_k|, \forall k$. This observation ascertains the above inequality.

Since $C_\tau, \tau \log \tau$ and $\tau \log K$ approach zero as $\tau \rightarrow 0$, we have $\lim_{\tau \rightarrow 0} S(X) = |X - Y_{k_0}| = r(X)$.

2D: Let the grid location X and the point source Y_k be represented by (x, y) and (x_k, y_k) respectively. We define $\phi_k^\tau(X)$ as

$$\phi_k^\tau(X) = \begin{cases} \frac{1}{\tau}; & x_k - \frac{\tau}{2} \leq x \leq x_k + \frac{\tau}{2}, \\ & y_k - \frac{\tau}{2} \leq y \leq y_k + \frac{\tau}{2}; \\ 0 & \text{otherwise} \end{cases}$$

such that it is square integrable to 1 and behaves like the square-root of the δ function centered at Y_k as τ tends to zero. Using the expression for the 2D Green's function and the relation 2.4, the Euclidean distance function is given by

$$S(X) = C_\tau - \tau \log \left(\sum_{k=1}^K \int_{\mathcal{B}_k^\tau(X)} K_0 \left(\frac{\|Z\|}{\tau} \right) dZ \right), \quad (2.15)$$

where $C_\tau = \tau \log(2\pi) + 3\tau \log \tau$ and the integral region $\mathcal{B}_k^\tau(X)$ equals

$$\mathcal{B}_k^\tau(X) = \left[x - x_k - \frac{\tau}{2}, x - x_k + \frac{\tau}{2} \right] \times \left[y - y_k - \frac{\tau}{2}, y - y_k + \frac{\tau}{2} \right]. \quad (2.16)$$

Defining

$$\alpha_k \equiv \begin{cases} 1 & \text{if } x > x_k; \\ -1 & \text{if } x < x_k \end{cases}$$

and

$$\beta_k \equiv \begin{cases} 1 & \text{if } y > y_k; \\ -1 & \text{if } y < y_k \end{cases}$$

for each k and closely following the arguments illustrated for the 1D case, we get

$$\begin{aligned} S(X) &\leq C_\tau - \tau \log \left\{ \tau K_0 \left(\frac{\|X_{1\tau} - Y_{k_0}\|}{\tau} \right) \right\} \\ &= C_\tau - \tau \log(\tau) - \tau \log \left\{ K_0 \left(\frac{\|X_{1\tau} - Y_{k_0}\|}{\tau} \right) \right\} \end{aligned} \quad (2.17)$$

for small values of τ , where $X_{1\tau} = (x + \alpha_k \frac{\tau}{2}, y + \beta_k \frac{\tau}{2})$. As in the 1D case, note that $\|X_{1\tau} - Y_{k_0}\| \geq \|Z\|$ for $Z \in \mathcal{B}_{k_0}$.

Using the relation $K_0(z) \geq \frac{\exp(-z)}{\sqrt{z}}$ when $z \geq 0.5$, we observe that

$$S(X) \leq C_\tau - \tau \log(\tau) + \tau \log \left\{ \sqrt{\frac{\|X_{1\tau} - Y_{k_0}\|}{\tau}} \right\} + \|X_{1\tau} - Y_{k_0}\| \quad (2.18)$$

as τ approaches zero.

If we let $X_{2\tau} = (x - \alpha_k \frac{\tau}{2}, y - \beta_k \frac{\tau}{2})$, then similarly to the 1D case we arrive at the inequality

$$\begin{aligned} S(X) &\geq C_\tau - \tau \log \left\{ \tau \sum_{k=1}^K K_0 \left(\frac{\|X_{2\tau} - Y_k\|}{\tau} \right) \right\} \\ &\geq C_\tau - \tau \log(\tau) - \tau \log \left\{ K K_0 \left(\frac{\|X_{2\tau} - Y_{k_0}\|}{\tau} \right) \right\} \\ &= C_\tau - \tau \log(\tau) - \tau \log(K) - \tau \log \left\{ K_0 \left(\frac{\|X_{2\tau} - Y_{k_0}\|}{\tau} \right) \right\} \end{aligned} \quad (2.19)$$

As $K_0(z) \leq \exp(-z)$ when $z \geq 1.5$, we get

$$S(X) \geq C_\tau - \tau \log(\tau) - \tau \log(K) + \|X_{2\tau} - Y_{k_0}\| \quad (2.20)$$

at small values of τ . Since $X_{1\tau}, X_{2\tau}$ approach X as $\tau \rightarrow 0$ and the rest of the terms tend to zero in the limit, we arrive at our desired result, namely $\lim_{\tau \rightarrow 0} S(X) = \|X - Y_{k_0}\| = r(X)$.

3D: Let the grid location X and the source point Y_k be denoted by $X = (x, y, z)$ and $Y_k = (x_k, y_k, z_k)$ respectively. To ensure square-integrability to 1 we define ϕ_k^τ as

$$\phi_k^\tau(X) = \begin{cases} \frac{1}{\tau^{\frac{3}{2}}}; & x_k - \frac{\tau}{2} \leq x \leq x_k + \frac{\tau}{2}, \\ & y_k - \frac{\tau}{2} \leq y \leq y_k + \frac{\tau}{2}, \\ & z_k - \frac{\tau}{2} \leq z \leq z_k + \frac{\tau}{2}, \\ 0 & \text{otherwise} \end{cases}$$

By exactly following the line of argument described for the 1D and the 2D case where we bound $S(X)$ above and below by functions which converge to the true Euclidean distance function $r(X)$ as τ tends to zero, we can establish the result $\lim_{\tau \rightarrow 0} S(X) = \|X - Y_{k_0}\| = r(X)$.

2.3. Closed-form solution and the error bound between the obtained and true Euclidean distance function. Based on the nature of the expression for the Green's function, it is worth accentuating the following *very* important point. Observe from above that the expression for Green's function G in either 1D, 2D or 3D takes the form

$$\lim_{\tau \rightarrow 0} \frac{\exp\left\{-\frac{\|X\|}{\tau}\right\}}{c\tau^d\|X\|^p} = 0, \text{ for } \|X\| \neq 0 \quad (2.21)$$

for c, d and p being constants greater than zero. In the limiting case of $\tau \rightarrow 0$, we see that if we define

$$\tilde{G}(X) \equiv C \exp\left(\frac{-\|X\|}{\tau}\right), \quad (2.22)$$

for some constant C , then

$$\lim_{\tau \rightarrow 0} |G(X) - \tilde{G}(X)| = 0, \text{ for } \|X\| \neq 0 \quad (2.23)$$

and furthermore, the convergence is *uniform* for $\|X\|$ away from zero. Therefore, $\tilde{G}(X)$ provides a very good approximation for the actual unbounded domain Green's function as $\tau \rightarrow 0$. For a fixed value of τ and X , the difference between the Green's functions is $O\left(\frac{\exp(-\frac{\|X\|}{\tau})}{\tau^2}\right)$ which is relatively insignificant for small values of τ and for all $X \neq 0$. Moreover, using \tilde{G} also avoids the singularity at the origin in the 2D and 3D case. The above observation motivates us to compute the solutions for ϕ by convolving with \tilde{G} instead of the actual Green's function G .

Furthermore, our proof technique used to manifest convergence of $S(X)$ to the true solution $r(X)$ —described in the preceding section—also encourages us to supplant the integral $\int_{B_k^\tau(X)} G(Z)dZ$ —obtained as a result of convolving the Green's function G with ϕ_k^τ —with $\tau^D G(X - Y_k)$ at small values of τ . Here D corresponds to the spatial dimension. This is a cogent approximation for the following reasons. Firstly, the integral region $B_k^\tau(X)$ is considered around $X - Y_k$ with its area/volume dwindling to zero as τ approaches zero (refer Equations 2.12 and 2.16). Hence we can replace the integral $\int_{B_k^\tau(X)} G(Z)dZ$ with its Riemann summation by assuming that $G(Z)$ is *constant* over $B_k^\tau(X)$ and equals the mid-point value $G(X - Y_k)$. Secondly, our proof explicitly corroborates that substituting the integral by either $\tau^D \sup_{Z \in B_k^\tau(X)} G(Z)$ or $\tau^D \inf_{Z \in B_k^\tau(X)} G(Z)$, we can still establish convergence to the true solution. Since $\inf_{Z \in B_k^\tau(X)} G(Z) \leq G(X - Y_k) \leq \sup_{Z \in B_k^\tau(X)} G(Z)$, our approximation is sound at small values of τ . Thirdly, it bestows upon us with a *closed-form* solution for ϕ as seen below.

These insights inspires us to solve for the scalar field ϕ as

$$\phi(X) \approx \left\{ \tau^D \tau^{-\gamma} C \sum_{k=1}^K \exp\left(\frac{-\|X - Y_k\|}{\tau}\right) \right\} \quad (2.24)$$

rather than via Equation 2.9. Here $\tau^{-\gamma}$ corresponds to the value of $\phi_k^\tau(Y_k)$, with γ determined by the spatial dimension. The approximate Euclidean distance function computed based on the relation 2.4 is given by

$$S(X) \approx (\gamma - D)\tau \log \tau - \tau \log C - \tau \log \left\{ \sum_{k=1}^K \exp \left(\frac{-\|X - Y_k\|}{\tau} \right) \right\}. \quad (2.25)$$

Since $(\gamma - D)\tau \log \tau$ and $\tau \log C$ are constants independent of X and converges to zero as $\tau \rightarrow 0$, they can be ignored while solving for S at small values of τ . Hence the scalar field $\phi(X)$ corresponding to the Euclidean distance function can be approximated by

$$\phi(X) \approx \sum_{k=1}^K \exp \left(\frac{-\|X - Y_k\|}{\tau} \right). \quad (2.26)$$

and the approximate Euclidean distance function equals

$$S(X) = -\tau \log \left\{ \sum_{k=1}^K \exp \left(\frac{-\|X - Y_k\|}{\tau} \right) \right\}. \quad (2.27)$$

We would like to underscore that the approximate function defined in Equation 2.26 possess all the desirable properties that we need. Firstly, we notice that as $\tau \rightarrow 0$, $\phi(Y_k) \rightarrow 1$ at the given point-set locations Y_k . Using the relation (2.4) we get $S(Y_k) \rightarrow 0$ as $\tau \rightarrow 0$ satisfying the initial conditions. Secondly for small values of τ , $\sum_{k=1}^K \exp \left(\frac{-\|X - Y_k\|}{\tau} \right)$ can be subrogated by $\exp \left(\frac{-r(X)}{\tau} \right)$ where $r(X)$ is the true Euclidean distance given by $r(X) = \min_k \|X - Y_k\|$. Hence

$$S(X) \approx -\tau \log \exp \left(\frac{-r(X)}{\tau} \right) = r(X). \quad (2.28)$$

Thirdly, $\phi(X)$ can be easily computed using the fast Fourier transform as discussed under the subsequent section. Hence for all practical, computational purposes we consider the function shown in Equation 2.26. The bound derived below between the approximate $S(X)$ and the true solution $r(X)$ also unveils the proximity between the computed and the actual Euclidean distance function.

Note from Equation 2.27 that

$$S(X) \leq -\tau \log \exp \left(\frac{-r(X)}{\tau} \right) = r(X). \quad (2.29)$$

Also we get

$$\begin{aligned} S(X) &\geq -\tau \log \left\{ K \exp \left(\frac{-r(X)}{\tau} \right) \right\} \\ &= -\tau \log K + r(X) \end{aligned} \quad (2.30)$$

and hence,

$$r(X) - S(X) \leq \tau \log K. \quad (2.31)$$

From Equations 2.29 and 2.31, we have

$$|r(X) - S(X)| \leq \tau \log K. \quad (2.32)$$

It is worth commenting that the bound $\tau \log K$ is actually very tight as (i) it scales only as the logarithm of the cardinality of the point-set (K) and (ii) it can be made arbitrarily small by choosing a small but non-zero value of τ .

TABLE 3.1
Approximate Euclidean distance function algorithm

1. Compute the function $f(X) = \exp\left(\frac{-\|X\|}{\tau}\right)$ at the grid locations.
2. Define the function $\delta_{kron}(X)$ which takes the value 1 at the point-set locations and 0 at other grid locations.
3. Compute the *FFT* of f and g , namely $F_{FFT}(U)$ and $G_{FFT}(U)$ respectively.
4. Compute the function $H(U) = F_{FFT}(U)G_{FFT}(U)$.
5. Compute the inverse *FFT* of $H(U)$ to obtain $\phi(X)$.
6. Take the logarithm of $\phi(X)$ and multiply it by $(-\tau)$ to recover the approximate Euclidean distance function.

3. Efficient computation of the approximate unsigned Euclidean distance function. We now provide a fast $O(N \log N)$ convolution-based method to compute the distance transform on a set of N grid locations $\{X_i, i = \{1, \dots, N\}\}$. The solution for $\phi(X)$ in Equation 2.26 at the grid locations can be represented as the *discrete convolution* between the functions

$$f(X) \equiv \exp\left(\frac{-\|X\|}{\tau}\right) \quad (3.1)$$

computed at the grid locations, with the function $g(X)$ which takes the value 1 at the point-set locations and 0 at other grid locations, i.e,

$$g(X) \equiv \sum_{k=1}^K \delta_{kron}(X - Y_k) \quad (3.2)$$

where,

$$\delta_{kron}(X - Y_k) \equiv \begin{cases} 1 & \text{if } X = Y_k; \\ 0 & \text{otherwise} \end{cases} \quad (3.3)$$

By the convolution theorem [3], a discrete convolution can be obtained as the inverse Fourier transform of the product of two individual transforms, which for two $O(N)$ sequences can be computed in $O(N \log N)$ time [5]. One just needs to compute the discrete Fourier transform (DFT) of the sampled version of the functions $f(X)$ and $g(X)$, compute their point-wise product and then compute the inverse discrete Fourier transform. Taking the logarithm of the inverse discrete Fourier transform and multiplying it by $(-\tau)$, gives the approximate Euclidean distance function. The algorithm is adumbrated in Table 3.1.

3.1. Computation of the approximate Euclidean distance function in higher dimensions. Our technique has a straightforward generalization to higher dimensions. Regardless of the spatial dimension, the approximate Euclidean distance function, S can be computed by exactly following the steps delineated in Table 3.1. It is worthwhile mentioning that computing the discrete Fourier transform using the *FFT* is always $O(N \log N)$ *irrespective* of the spatial dimension. Hence, for all dimensions, S can be computed at the given N grid points in $O(N \log N)$. This speaks for the scalability of our technique, which is generally not the case with other methods, for example KD-Trees [6] *.

*Though the actual number of grid points(N) increases with dimension, the solution is always $O(N \log N)$ in the number of grid points.

3.2. Numerical issues. In principle, we should be able to apply our technique at very small values of τ and obtain highly accurate results. But we noticed that a naïve double precision-based implementation tends to deteriorate for τ values very close to zero. This is due to the fact that at small values of τ , $f(X)$ drops off very quickly and hence for grid locations which are far away from the point-set, the convolution done using FFT may not be accurate. To this end, we turned to the GNU MPFR multiple-precision arithmetic library which provides arbitrary precision arithmetic with correct rounding [7]. MPFR is based on the GNU multiple-precision library (GMP) [18]. It enabled us to run our technique at very small values of τ giving highly accurate results. We corroborate our claim and demonstrate the usefulness of our method with the set of experiments described under Section 6.

3.3. Exact computational complexity. More the number of precision bits p used in the GNU MPFR library, better is the accuracy of our technique, as the error incurred in the floating point operations can be bounded by $O(2^{-p})$. But using more bits has an adverse effect of slowing down the running time. The $O(N \log N)$ time complexity of the FFT algorithm [5] for an $O(N)$ length sequence represents only the number of floating-point operations involved, barring any numerical accuracy. The accuracy of the FFT algorithm and our technique entirely depends on the number of precision bits used for computing elementary functions like exp, log, sin and cos and hence should be taken into account while calculating the exact time complexity. If p precision bits are used, these elementary functions can be computed in $O(M(p) \log p)$ [4, 14, 17], where $M(p)$ is the computational complexity for multiplying two p -digit numbers. The Schönhage-Strassen algorithm [15] gives an asymptotic upper bound for $M(p)$ with a run-time bit complexity of $M(p) = O(p \log p \log \log p)$. The actual running time of our algorithm—while taking these p precision bits into account—for computing S at the given N grid locations is then $O(N \log(N)p(\log p)^2 \log(\log p))$ bit-wise operations.

4. Fast computation of signed distance functions. The solution for the approximate Euclidean distance function in Equation 2.27 is lacking in one respect: there is no information on the sign of the distance. This is to be expected since the distance function was obtained only from a set of *points* Y and not a curve or surface. We now describe a new method for computing the signed distance function in 2D using winding numbers and in 3D using the topological degree.

4.1. Computing winding numbers. Assume that we have a closed, parametric curve $\{x^{(1)}(t), x^{(2)}(t)\}$, $t \in [0, 1]$. We seek to determine if a grid location in the set $\{X_i \in \mathbb{R}^2, i \in \{1, \dots, N\}\}$ is inside the closed curve. The winding number is the number of times the curve winds around the point X_i (if at all) with counterclockwise turns counted as positive and clockwise turns as negative. If a point is inside the curve, the winding number is a non-zero integer. If the point is outside the curve, the winding number is zero. If we can efficiently compute the winding number for all points on a grid w.r.t. to a curve, then we would have the sign information (inside/outside) for all the points. We now describe a fast algorithm to achieve this goal.

If the curve is C^1 , then the angle $\theta(t)$ of the curve is continuous and differentiable and $d\theta(t) = \left(\frac{x^{(1)}\dot{x}^{(2)} - x^{(2)}\dot{x}^{(1)}}{\|x\|^2} \right) dt$. Since we need to determine whether the curve winds around each of the points $X_i, i \in \{1, \dots, N\}$, define $(\hat{x}_i^{(1)}, \hat{x}_i^{(2)}) \equiv (x^{(1)} - X_i^{(1)}, x^{(2)} - X_i^{(2)})$.

$X_i^{(2)}$), $\forall i$. Then the winding numbers for the grid point X_i is

$$\mu_i = \frac{1}{2\pi} \oint_C \left(\frac{\hat{x}_i^{(1)} \dot{\hat{x}}_i^{(2)} - \hat{x}_i^{(2)} \dot{\hat{x}}_i^{(1)}}{\|\hat{x}_i\|^2} \right) dt, \quad \forall i \in \{1, \dots, N\}. \quad (4.1)$$

As it stands, we cannot actually compute the winding numbers without performing the integral in Equation 4.1. To this end, we discretize the curve and produce a sequence of points $\{Y_k \in \mathbb{R}^2, k \in \{1, \dots, K\}\}$ with the understanding that the curve is closed and therefore the “next” point after Y_K is Y_1 . (The winding number property holds for piecewise continuous curves as well.) The integral in Equation 4.1 becomes a discrete summation and we get

$$\mu_i = \frac{1}{2\pi} \sum_{k=1}^K \frac{\left(Y_k^{(1)} - X_i^{(1)} \right) \left(Y_{k+1}^{(2)} - Y_k^{(2)} \right) - \left(Y_k^{(2)} - X_i^{(2)} \right) \left(Y_{k+1}^{(1)} - Y_k^{(1)} \right)}{\|Y_k - X_i\|^2} \quad (4.2)$$

$\forall i \in \{1, \dots, N\}$, where the notation $Y_{k+1}^{(\cdot)}$ denotes that $Y_{k+1}^{(\cdot)} = Y_{k+1}^{(\cdot)}$ for $k \in \{1, \dots, K-1\}$ and $Y_{K+1}^{(\cdot)} = Y_1^{(\cdot)}$. We can simplify the notation in Equation 4.2 (and obtain a measure of conceptual clarity as well) by defining the “tangent” vector $\{Z_k, k = \{1, \dots, K\}\}$ as

$$Z_k^{(\cdot)} = Y_{k+1}^{(\cdot)} - Y_k^{(\cdot)}, \quad k \in \{1, \dots, K\} \quad (4.3)$$

with the (\cdot) symbol indicating either coordinate. Using the tangent vector Z_k , we rewrite Equation 4.2 as

$$\mu_i = \frac{1}{2\pi} \sum_{k=1}^K \frac{\left(Y_k^{(1)} - X_i^{(1)} \right) Z_k^{(2)} - \left(Y_k^{(2)} - X_i^{(2)} \right) Z_k^{(1)}}{\|Y_k - X_i\|^2}, \quad \forall i \in \{1, \dots, N\} \quad (4.4)$$

We now make the somewhat surprising observation that μ_i in Equation 4.4 is a sum of two discrete convolutions. The first convolution is between two functions $f_{cr}(X) \equiv f_c(X)f_r(X)$ and $g_2(X) = \sum_{k=1}^K Z_k^{(2)} \delta_{\text{kron}}(X - Y_k)$. The second convolution is between two functions $f_{sr}(X) \equiv f_s(X)f_r(X)$ and $g_1(X) \equiv \sum_{k=1}^K Z_k^{(1)} \delta_{\text{kron}}(X - Y_k)$. The Kronecker delta function $\delta_{\text{kron}}(X - Y_k)$ is defined Equation 3.3. The functions $f_c(X)$, $f_s(X)$ and $f_r(X)$ are defined as

$$f_c(X) \equiv \frac{X^{(1)}}{\|X\|}, \quad f_s(X) \equiv \frac{X^{(2)}}{\|X\|}, \quad \text{and} \quad (4.5)$$

$$f_r(X) \equiv \frac{1}{\|X\|} \quad (4.6)$$

with the understanding that $f_c(0) = f_s(0) = f_r(0) = 0$. Here we have abused notation somewhat and let $X^{(1)} (X^{(2)})$ denote the $x (y)$ -coordinate of the grid point X . Armed with these relationships, we rewrite (4.4) to get

$$\mu(X) = \frac{1}{2\pi} [-f_{cr}(X) * g_2(X) + f_{sr}(X) * g_1(X)] \quad (4.7)$$

which can be computed in $O(N \log N)$ time using FFT-based convolution *simultaneously* for all the N grid points $\{X_i, i = \{1, \dots, N\}\}$.

4.2. Computing topological degree. The winding number concept for 2D admits a straight forward generalization to 3D and higher dimensions. The equivalent concept is the topological degree which is based on normalized flux computations. Assume that we have an oriented surface in 3D [8] which is represented as a set of K triangles. The k^{th} triangle has an outward pointing normal P_k and this can easily be obtained once the surface is oriented. (We vectorize the edge of each triangle. Since triangles share edges, if the surface can be oriented, then there's a consistent way of lending direction to each triangle edge. The triangle normal is merely the cross-product of the triangle vector edges.) We pick a convenient triangle center (the triangle incenter for instance) for each triangle and call it Y_k . The normalized flux (which is very closely related to the topological degree) [1] determines the ratio of the outward flux from a point X_i treated as the origin. If X_i is outside the enclosed surface, then the total outward flux is zero. If the point is inside, the outward normalized flux will be non-zero and positive.

The normalized flux for a point X_i is

$$\mu_i = \frac{1}{4\pi} \sum_{k=1}^K \frac{\langle (Y_k - X_i), P_k \rangle}{\|Y_k - X_i\|^3}. \quad (4.8)$$

This can be written in the form of convolutions. To see this, we write Equation 4.8 in component form:

$$\mu_i = \frac{1}{4\pi} \sum_{k=1}^K \frac{(Y_k^{(1)} - X_i^{(1)})P_k^{(1)} + (Y_k^{(2)} - X_i^{(2)})P_k^{(2)} + (Y_k^{(3)} - X_i^{(3)})P_k^{(3)}}{\|Y_k - X_i\|^3} \quad (4.9)$$

which can be simplified as

$$\mu(X) = -\frac{1}{4\pi} (f_1(X) * g_1(X) + f_2(X) * g_2(X) + f_3(X) * g_3(X)) \quad (4.10)$$

where $f_{(\cdot)}(X) \equiv \frac{X^{(\cdot)}}{\|X\|^3}$ and $g_{(\cdot)}(X) \equiv \sum_{k=1}^K P_k^{(\cdot)} \delta_{\text{kron}}(X - Y_k)$ where the Kronecker delta function $\delta_{\text{kron}}(X - Y_k)$ is defined Equation 3.3. This can be computed in $O(N \log N)$ time using FFT-based convolution for all the N grid points X_i .

For the sake of clarity we explicitly show the generalization of the winding number to the topological degree by rewriting some of the calculations involved in computing the winding number. Recall that for every point Y_k on the discretized curve, we defined its tangent vector Z_k as in equation (4.3). The *outward pointing normal* $P_k = (P_k^{(1)}, P_k^{(2)})$, at the point Y_k (P_k will point outwards provided Y_1, Y_2, \dots, Y_k are taken in the anti-clockwise order), is given by $P_k^{(1)} = Z_k^{(2)}$, $P_k^{(2)} = -Z_k^{(1)}$. Using the normal vector P_k , equation (4.4) can be rewritten as

$$\mu_i = \frac{1}{2\pi} \sum_{k=1}^K \frac{\langle (Y_k - X_i), P_k \rangle}{\|Y_k - X_i\|^2}. \quad (4.11)$$

Notice the similarity between equations (4.11) and (4.8). This manifests that the topological degree is just a generalization of the winding number concept.

We have thus demonstrated that the sign component of the Euclidean distance function can be separately computed (without knowledge of the distance) in parallel in $O(N \log N)$ on a regular 2D and 3D grid.

5. Fast computation of the derivatives of the distance function. Just as the approximate Euclidean distance function $S(X)$ can be efficiently computed in $O(N \log N)$, so can the derivatives. This is important because fast computation of the derivatives of $S(X)$ on a regular grid can be very useful in curvature computations. Below, we detail how this can be achieved. We begin with the gradients and for illustration purposes, the derivations are performed in 2D:

$$S_x(X) = \frac{\sum_{k=1}^K \frac{X^{(1)} - Y_k^{(1)}}{\|X - Y_k\|} \exp\left(-\frac{\|X - Y_k\|}{\tau}\right)}{\sum_{k=1}^K \exp\left(-\frac{\|X - Y_k\|}{\tau}\right)}. \quad (5.1)$$

A similar expression can be obtained for $S_y(X)$. These first derivatives can be rewritten as discrete convolutions:

$$S_x(X) = \frac{f_c(X)f(X)*g(X)}{f(X)*g(X)}, \quad S_y(X) = \frac{f_s(X)f(X)*g(X)}{f(X)*g(X)}, \quad (5.2)$$

where $f_c(X)$ and $f_s(X)$ are as defined in Equation 4.5 and $f(X)$ and $g(X)$ are given in Equations 3.1 and 3.2 respectively.

The second derivative formulas are somewhat involved. Rather than hammer out the algebra in a turgid manner, we merely present the final expressions—all discrete convolutions—for the three second derivatives in 2D:

$$S_{xx}(X) = \frac{[-\frac{1}{\tau}f_c^2(X) + f_s^2(X)f_r(X)]f(X)*g(X)}{f(X)*g(X)} + \frac{1}{\tau}(S_x)^2(X), \quad (5.3)$$

$$S_{yy}(X) = \frac{[-\frac{1}{\tau}f_s^2(X) + f_c^2(X)f_r(X)]f(X)*g(X)}{f(X)*g(X)} + \frac{1}{\tau}(S_y)^2(X), \text{ and} \quad (5.4)$$

$$S_{xy}(X) = \frac{-[\frac{1}{\tau} + f_r(X)]f_c(X)f_s(X)f(X)*g(X)}{f(X)*g(X)} + \frac{1}{\tau}S_x(X)S_y(X) \quad (5.5)$$

where $f_r(X)$ is as defined in Equation 4.6.

Since we can efficiently compute the first and second derivatives of the approximate Euclidean distance function everywhere on a regular grid, we can also compute derived quantities such as curvature (Gaussian, mean and principal curvatures) for the two-dimensional surface $S(X)$ computed at the grid locations X . In Section 6, we visualize the derivatives for certain shape silhouettes.

5.1. Convergence analysis for the derivatives. We now show convergence of the derivatives (S_x, S_y) obtained via Equation 5.1 to their true value as $\tau \rightarrow 0$. Recall that the true distance function is not differentiable at the point-source locations $\{Y_k\}_{k=1}^K$ and on the Voronoi boundaries which corresponds to grid locations which are equidistant from two or more point sources. Hence it is meaningful to speak about convergence only for grid locations whose closest source point can be uniquely determined.

For illustration purposes we show the analysis in 2D. Let Y_{k_0} denote the unique closest source point for the grid location X_0 , i.e., $\|Y_{k_0} - X_0\| < \|Y_k - X_0\|, \forall k \neq k_0$. Then its true derivatives are given by

$$S_x^*(X_0) = \frac{X_0^{(1)} - Y_{k_0}^{(1)}}{\|X_0 - Y_{k_0}\|}, \quad S_y^*(X_0) = \frac{X_0^{(2)} - Y_{k_0}^{(2)}}{\|X_0 - Y_{k_0}\|}. \quad (5.6)$$

Multiplying and dividing the Equation 5.1 by $\exp\left(\frac{\|X_0 - Y_{k_0}\|}{\tau}\right)$, we get

$$S_x(X_0) = \frac{\frac{X_0^{(1)} - Y_{k_0}^{(1)}}{\|X_0 - Y_{k_0}\|} + \sum_{k=1, k \neq k_0}^K \frac{X_0^{(1)} - Y_k^{(1)}}{\|X_0 - Y_k\|} \exp\left(-\frac{\gamma_k}{\tau}\right)}{1 + \sum_{k=1, k \neq k_0}^K \exp\left(-\frac{\gamma_k}{\tau}\right)} \quad (5.7)$$

where $\gamma_k = \|X_0 - Y_k\| - \|X_0 - Y_{k_0}\|$. Since $\gamma_k > 0, \forall k \neq k_0$, it follows that $\lim_{\tau \rightarrow 0} \exp\left(-\frac{\gamma_k}{\tau}\right) = 0, \forall k \neq k_0$. Since all the other terms in Equation 5.7 are independent of τ , we get $\lim_{\tau \rightarrow 0} S_x(X_0) = S_x^*(X_0)$. The convergence analysis for $S_y(X_0)$ follows along similar lines.

Furthermore, the gradient magnitude $\|\nabla S(X)\|$ for any non-zero value of τ will be strictly less than its true value $\sqrt{(S_x^*(X))^2 + (S_y^*(X))^2} = 1$. To see this consider Equation 5.1 and for the sake of convenience define $\alpha_k = \frac{X^{(1)} - Y_k^{(1)}}{\|X - Y_k\|}$, $\beta_k = \frac{X^{(2)} - Y_k^{(2)}}{\|X - Y_k\|}$ and $E_k = \exp\left(-\frac{\|X - Y_k\|}{\tau}\right)$. Since $\alpha_k^2 + \beta_k^2 = 1, \forall k$, we get

$$\|\nabla S(X)\|^2 = \frac{\sum_{k=1}^K E_k^2 + 2 \sum_{k=1}^K \sum_{l>k}^K (\alpha_k \alpha_l + \beta_k \beta_l) E_k E_l}{\sum_{k=1}^K E_k^2 + 2 \sum_{k=1}^K \sum_{l>k}^K E_k E_l}. \quad (5.8)$$

Using the Cauchy-Schwarz inequality, we have

$$|\alpha_k \alpha_l + \beta_k \beta_l| < \sqrt{\alpha_k^2 + \beta_k^2} \sqrt{\alpha_l^2 + \beta_l^2} = 1. \quad (5.9)$$

It is then easy to see that $\|\nabla S(X)\| < 1$. We provide experimental evidence in the subsequent section to corroborate this fact. Nevertheless, the magnitude value converges to 1 as $\tau \rightarrow 0$ at all the grid locations barring the point-sources and the Voronoi boundaries, as the gradients themselves converge to their true value.

6. Experiments. In this section we show the usefulness of our linear approach to computing Euclidean distance functions by running it on a bounded 2D and 3D grid. As we discussed before, in order improve the computational accuracy of our technique we are forced to go beyond the precision supported by the double floating-point numbers (64 bits) and resort to arbitrary precision packages like GNU multiple-precision library (GMP) [18] and MPFR [7]. For the following experiments we used $p = 512$ precision bits.

6.1. 2D Experiments. Example 1: We begin by demonstrating the effect of τ on our method and evince that as $\tau \rightarrow 0$, the accuracy our method does improve significantly. To this end, we considered a 2D grid consisting of points between $(-0.121, -0.121)$ and $(0.121, 0.121)$ with a grid width of $\frac{1}{2^9}$. The total number of grid points is then $N = 125 \times 125 = 15,625$. We ran 1000 experiments each time randomly choosing 5000 grid locations as data points (point-set), for 9 different values of τ ranging from 5×10^{-5} to 4.5×10^{-4} in steps of 5×10^{-5} . For each run and each value of τ , we calculated the percentage error as

$$\text{error} = \frac{100}{N} \sum_{i=1}^N \frac{\Delta_i}{D_i}, \quad (6.1)$$

where D_i and Δ_i are respectively the actual distance and the absolute difference of the computed distance to the actual distance at the i^{th} grid point. Figure 6.1

shows the *mean* percentage error at each value of τ . The *maximum* value of the error at each value of τ is summarized in table 6.1. The error is less than 0.6% at $\tau = 0.00005$ demonstrating the algorithm's ability to compute accurate Euclidean distance functions.

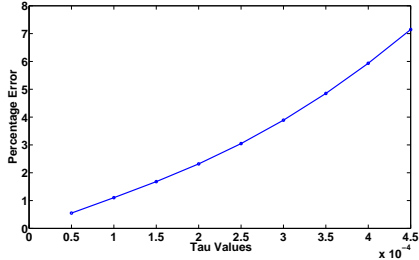


FIGURE 6.1. *Percentage error versus τ in 1000 2D experiments.*

τ	Maximum error
0.00005	0.5728%
0.0001	1.1482%
0.00015	1.7461%
0.0002	2.4046%
0.00025	3.1550%
0.0003	4.0146%
0.00035	4.9959%
0.0004	6.1033%
0.00045	7.3380%

TABLE 6.1
Maximum percentage error for different values of τ in 1000 2D experiments.

Example 2: We then executed our algorithm on a set of 2D shape silhouettes [16][†]. The grid size is $-0.125 \leq x \leq 0.125$ and $-0.125 \leq y \leq 0.125$ with a grid width of $\frac{1}{2^{10}}$. The number of grid locations equals $N = 257 \times 257 = 66,049$. We set τ for our method at 0.0003. For the sake of comparison, we ran the fast sweeping method for 10 iterations sufficient enough for it to converge. The percentage error calculated according to Equation 6.1 for both our method and fast sweeping in comparison to the true Euclidean distance function for each of these shapes are adumbrated in Table 6.2.

The true Euclidean distance function contour plots and those obtained from our method and fast sweeping are delineated in Figure 6.2.

In order to differentiate between the grid locations that are either inside or outside each shape, we computed the winding number for all the grid points *simultaneously* in $O(N \log N)$ using our convolution-based winding number method. Grid points with a winding number value greater than 0 after rounding were marked as interior points.

[†]We thank Kaleem Siddiqi for providing us the set of 2D shape silhouettes used in this paper.

Shape	Our linear method	Fast sweeping
Hand	2.182%	2.572%
Horse	2.597%	2.549%
Bird	2.116%	2.347%

TABLE 6.2

Percentage error for the Euclidean distance function computed using the grid points of these silhouettes as data points

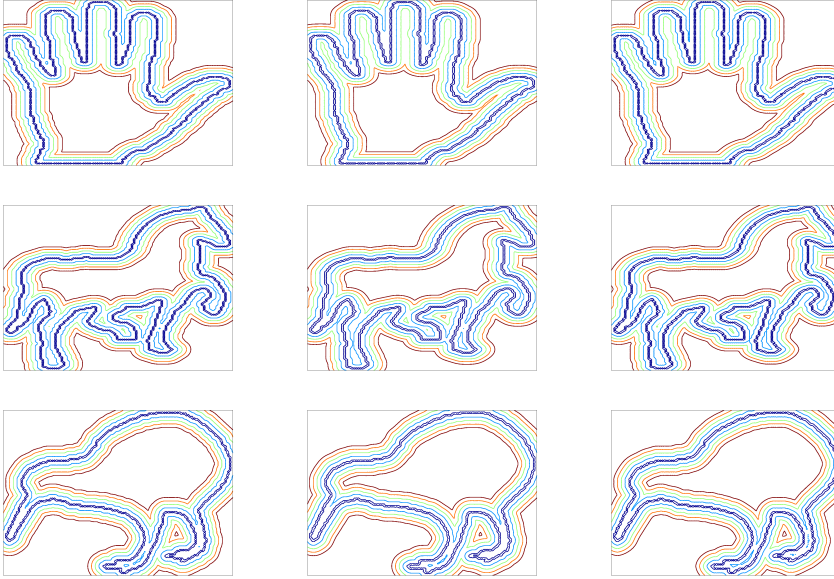


FIGURE 6.2. Contour plots: (i) Left: True Euclidean distance function, (ii) Center: Our method, (iii) Right: Fast sweeping

In the left part of Figure 6.3 we visualize the vector fields (S_x, S_y) for all the interior points (marked in blue). We see that our convolution-based technique for computing the winding number separates the interior grid points from the exterior with almost zero error. In the right part of Figure 6.3 we plot the distribution of the winding number values computed over all the interior and the exterior locations. Observe that for almost all the grid points, the winding number values are close to *binary*, i.e either 0 or 1, with a value of 0 marking the exterior points (as the curve doesn't wind around them) and 1 representing interior locations. A zoomed version of the quiver plot is shown in Figure 6.4.

In the left part of Figure 6.5, we picturize the distribution of the gradient magnitude ($\|\nabla S\|$) values. Since we don't solve for the true distance function S and rather approximate it by Equation 2.27, the magnitude of the gradients (S_x, S_y) obtained via Equation 5.1 may not necessarily satisfy the Hamilton-Jacobi equation 1.2. Their distribution values portrayed in Figure 6.5 manifests it. The reformulation of the derivatives given in Equation 5.7 drives this point home. Nevertheless, we do observe that most of the gradient magnitude values (about 90%) are greater than 0.9. Also

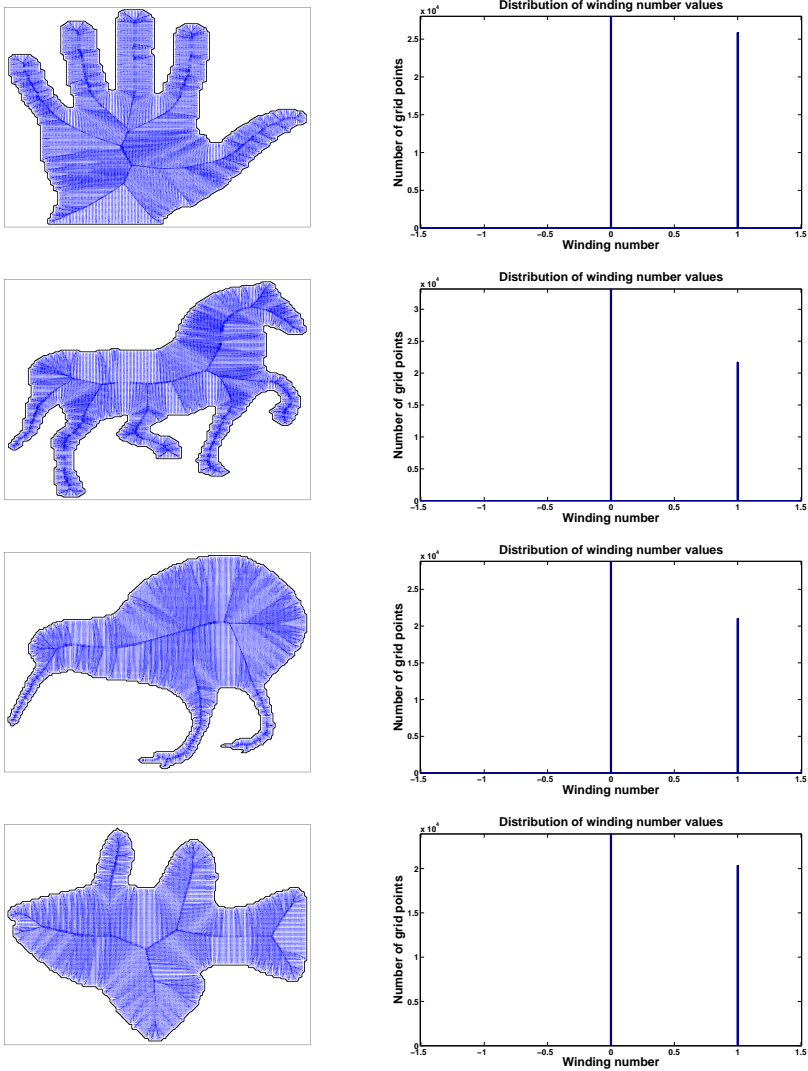


FIGURE 6.3. (i) Left: Quiver plot of $\nabla S = (S_x, S_y)$ for a set of silhouette shapes (best viewed in color), (ii) Right: Distribution of winding numbers

notice that all the gradient magnitudes are less than 1, as we evinced in Section 5.1.

In the right part of Figure 6.5, we visualize the gradient magnitude values as an image plot in tints of gray. Grid locations whose gradient magnitude values are in proximity to 1 are marked as white and black indicates grid points whose gradient magnitude values are closer to its minimum value on the grid. From these image plots it is quite clear that the grid points which are either too close to the point-sources or lie along the medial axis (corresponding to the Voronoi boundaries for these shapes) incur maximum errors in their gradient magnitude values. As these grid locations are almost equidistant from multiple point-sources, many of them contribute substantially to the summation value $\exp\left(-\frac{\|X-Y_k\|}{\tau}\right)$ instead of just the nearest one and hence the induced error is relatively high. Interestingly, it might be possible to actually

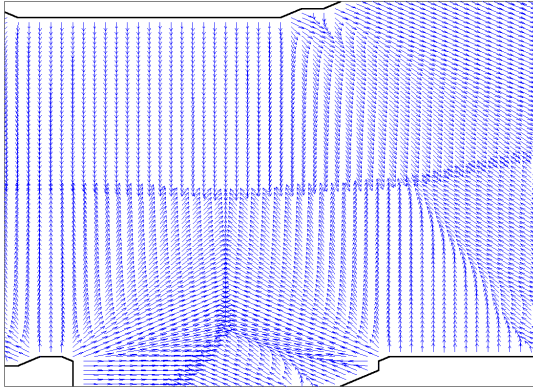


FIGURE 6.4. *Zoomed quiver plot*

leverage these inaccuracies for something good as they might aid in the medial axis computation. Notice that, it is fairly an easy task to trace the medial axis from these image plots. We are currently investigating whether this can be achieved.

6.2. 3D Experiments. Example 3: We also compared our Euclidean distance function algorithm with the fast sweeping method [20] and the exact Euclidean distance on the “Dragon” point-set obtained from the Stanford 3D Scanning Repository[‡]. The common grid was $-0.117 \leq x \leq 0.117$, $-0.086 \leq y \leq 0.086$ and $-0.047 \leq z \leq 0.047$ with a grid width of $\frac{1}{2^8}$. We ran our approach at $\tau = 0.0004$ and ran the fast sweeping method for 15 iterations which is sufficient for the Gauss-Seidel iterations to converge. We then calculated the percentage error for both these techniques according to Equation 6.1. While the average percentage error for our approach when compared to the true distance function was just **1.306%**, the average percentage error in the fast sweeping method was 6.84%. Our FFT-based approach does not begin by discretizing the spatial differential operator as is the case with the fast marching and fast sweeping methods and this could help account for the increased accuracy.

The isosurface obtained by connecting the grid points at a distance of 0.005 from the point set, determined by the true Euclidean distance function, our algorithm and fast sweeping are shown in Figure 6.6. The similarity between the plots provides anecdotal visual evidence for the usefulness of our approach.

Example 4: Next, to demonstrate the efficacy of our convolution-based technique for computing the topological degree, we ran the following experiments in 3D. The grid was confined to the region $-0.125 \leq x \leq 0.125$, $-0.125 \leq y \leq 0.125$ and $-0.125 \leq z \leq 0.125$ with a grid width of $\frac{1}{2^8}$. The number of grid points was $N = 274,625$. Given a set of points sampled from the surface of a 3D object, we triangulated the surface using some of the built-in MATLAB[®] routines. We consider the incenter of each triangle to represent the data points $\{Y_k\}_{k=1}^K$. The normal P_k for each triangle

[‡]This dataset is available at <http://graphics.stanford.edu/data/3Dscanrep/>.

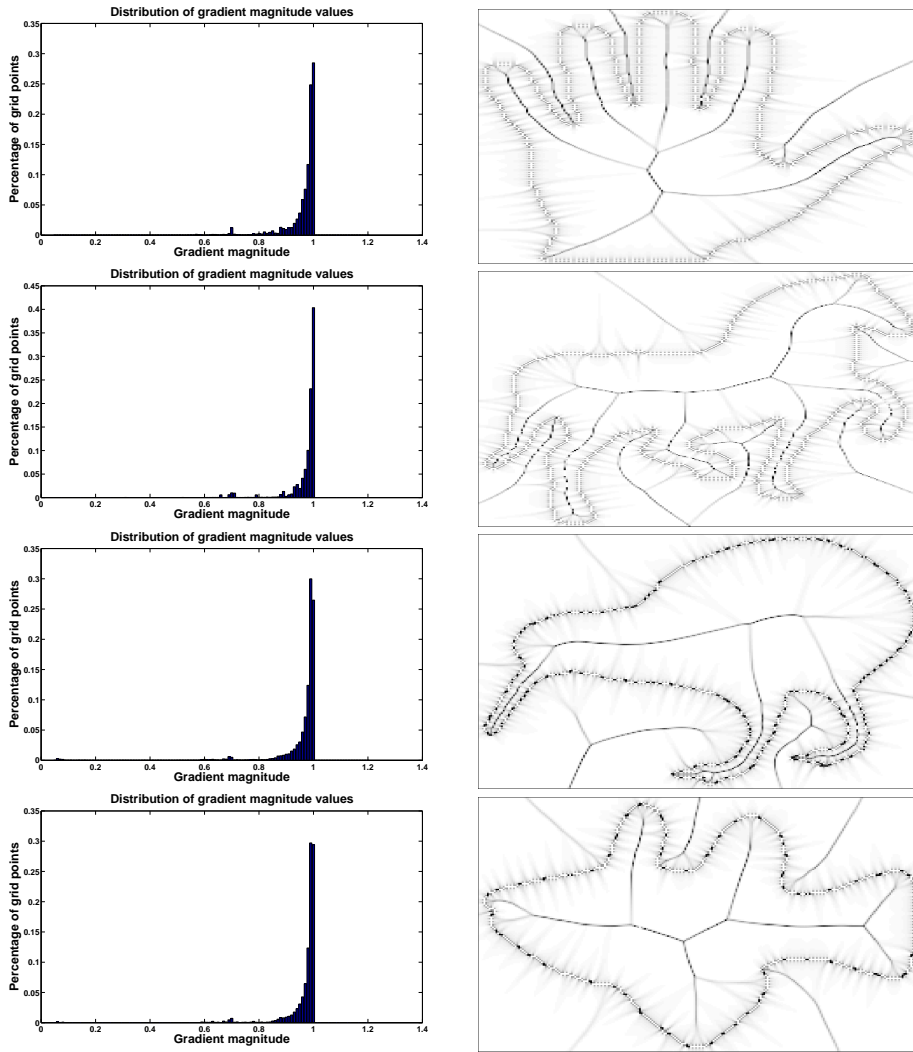


FIGURE 6.5. Gradient magnitude ($\|\nabla S\|$) (i) Left: Distribution, (ii) Right: Image plot

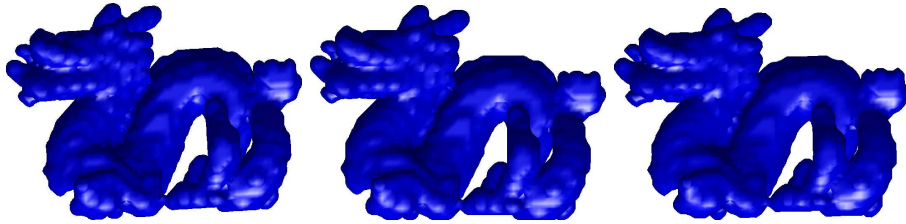


FIGURE 6.6. Isosurfaces: (i) Left: Actual Euclidean distance function, (ii) Center: Our algorithm and (iii) Right: Fast sweeping

can be computed from the cross-product of the triangle vector edges. The direction of the normal vector was determined by taking the dot product between the position vector \vec{Y}_k and the normal vector \vec{P}_k . For negative dot products, \vec{P}_k was negated to

obtain a outward pointing normal vector. We then computed the topological degree for all the N grid locations *simultaneously* in $O(N \log N)$ by running our convolution-based algorithm. Grid locations where the topological degree value exceeded 0.7 were marked as points lying inside the given 3D object. Figure 6.7 shows the interior points for the three 3D objects—cylinder, cube and sphere (left to right).

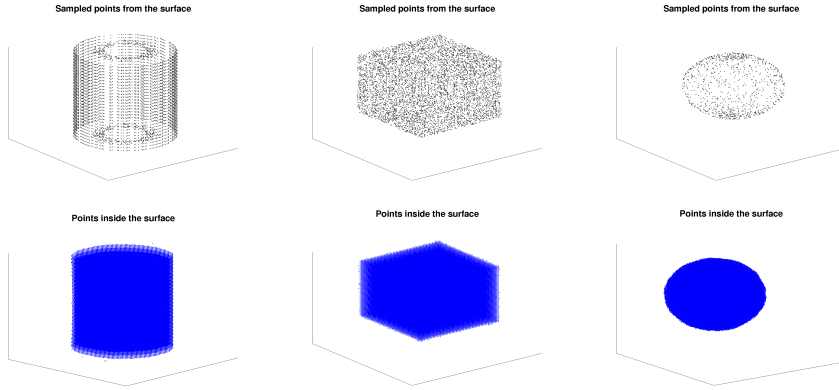


FIGURE 6.7. *Topological Degree:* (i) Top: Sampled points from the surface, (ii) Bottom: Grid points lying inside the surface (marked as blue)

7. Conclusion. In this work, we furnished a linear, variational formalism for the Euclidean distance function problem where we computed solutions on a bounded 2D and 3D grid. We posed a specific variational problem and evinced that the solution to its linear Euler-Lagrange equation at small values of τ can be used to obtain the Euclidean distance function. The intriguing aspect of our approach is that the non-linear Hamilton-Jacobi equation is embedded inside a *linear* equation and the solution is derived in the limiting case of $\tau \rightarrow 0$. We initially derived the solution for ϕ satisfying the Euler-Lagrange equation via the Green's function approach and later approximated it with a closed-form solution, the major advantage being that the closed-form solution is representable as a discrete convolution which can be efficiently computed in $O(N \log N)$ using FFT. The Euclidean distance is finally recovered from its exponent. Since the scalar field ϕ is computed for a small but non-zero τ , the obtained Euclidean distance function is an approximation. We derived analytic bounds for the error of the approximation for a given value of τ and provided proofs of convergence to the true distance function as $\tau \rightarrow 0$. The differentiability of our solution endows us to compute the gradients and curvature quantities of the distance function S in closed-form, also written as convolutions. Finally, we demonstrated how our discrete convolution-based technique for computing the winding number in 2D and the topological degree in 3D are useful in determining the sign of the distance function.

While Hamilton-Jacobi solvers have gone beyond the eikonal equation and regular grids—by providing efficient solutions even for the more general static Hamilton-Jacobi equation on irregular grids [11, 9, 10]—in the current work we restrict ourselves only to computing the Euclidean distance function on regular grids. In the future, we would like to follow the pioneering works of the fast marching [13] and fast sweeping [20] methods and try to extend our linear formalism even to irregular grids.

REFERENCES

- [1] O. Aberth, *Precise numerical methods using C++*, Academic Press, 1998.
- [2] M. Abramowitz and I.A. Stegun, *Handbook of Mathematical Functions with Formulas, Graphs, and Mathematical Tables*, Government Printing Office, USA, 1964.
- [3] R.N. Bracewell, *The Fourier Transform and its Applications*, 3rd ed., McGraw-Hill Science and Engineering, 1999.
- [4] R.P. Brent, *Fast multiple-precision evaluation of elementary functions*, Journal of the ACM **23** (1976), 242–251.
- [5] J.W. Cooley and J.W. Tukey, *An algorithm for the machine calculation of complex Fourier series*, Mathematics of Computation **19** (1965), no. 90, 297–301.
- [6] M. de Berg, O. Cheong, M. van Kreveld, and M. Overmars, *Computational Geometry: Algorithms and Applications*, Springer, 2008.
- [7] L. Fousse, G. Hanrot, V. Lefèvre, P. Pélissier, and P. Zimmermann, *MPFR: A multiple-precision binary floating-point library with correct rounding*, ACM Trans. Math. Software **33** (2007), 1–15.
- [8] A. Gray, *Modern differential geometry of curves and surfaces with mathematica*, 2nd ed., CRC Press, 1997.
- [9] Y.-T. Zhang J. Qian and H.K. Zhao, *Fast sweeping methods for eikonal equations on triangular meshes*, SIAM Journal on Numerical Analysis **45** (2007), no. 1, 83–107.
- [10] C.-Y. Kao, S.J. Osher, and J. Qian, *Legendre-transform-based fast sweeping methods for static Hamilton-Jacobi equations on triangulated meshes*, Journal of Computational Physics **227** (2008), 10209–10225.
- [11] C.-Y. Kao, S.J. Osher, and Y.-H. Tsai, *Fast sweeping methods for static Hamilton-Jacobi equations*, SIAM Journal on Numerical Analysis **42** (2004), no. 6, 2612–2632.
- [12] S.J. Osher and R.P. Fedkiw, *Level Set Methods and Dynamic Implicit Surfaces*, Springer, October 2002.
- [13] S.J. Osher and J.A. Sethian, *Fronts propagating with curvature dependent speed: algorithms based on Hamilton-Jacobi formulations*, Journal of Computational Physics **79** (1988), no. 1, 12–49.
- [14] T. Sasaki and Y. Kanada, *Practically fast multiple-precision evaluation of $\log(x)$* , Journal of Information Processing **5** (1982), 247–250.
- [15] A. Schönhage and V. Strassen, *Schnelle multiplikation großer zahlen*, Computing **7** (1971), 281–292.
- [16] K. Siddiqi, A. Tannenbaum, and S.W. Zucker, *A Hamiltonian approach to the eikonal equation*, Energy Minimization Methods in Computer Vision and Pattern Recognition (EMMCVPR), vol. LNCS 1654, Springer-Verlag, 1999, pp. 1–13.
- [17] D.M. Smith, *Efficient multiple-precision evaluation of elementary functions*, Mathematics of Computation **52** (1989), no. 185, 131–134.
- [18] G. Torbjörn and *et al.*, *GNU multiple precision arithmetic library 5.0.1*, June 2010.
- [19] L. Yatziv, A. Bartesaghi, and G. Sapiro, *$O(N)$ implementation of the fast marching algorithm*, J. Comput. Phys. **212** (2006), no. 2, 393–399.
- [20] H.K. Zhao, *A fast sweeping method for eikonal equations*, Mathematics of Computation (2005), 603–627.